

## Photoneutron Cross Sections in He, N, O, F, Ne, and A<sup>†</sup>

G. A. FERGUSON, J. HALPERN, R. NATHANS, AND P. F. YERGIN  
*University of Pennsylvania, Philadelphia, Pennsylvania*

(Received April 1, 1954)

The direct detection of neutrons from  $(\gamma, n)$  reactions induced by betatron bremsstrahlung has been applied to cross-section determinations using gaseous targets at approximately 100 atmospheres pressure. Results from oxygen are consistent with other determinations. The remaining elements represent new results and show the familiar giant dipole resonance for the photoneutron process. Parameters of the resonances are determined and related to the systematic behavior previously reported for other elements.

### INTRODUCTION

STUDIES of the energy dependence of the photoneutron cross sections for light elements have been a useful tool in exploring the nucleon-nucleon interaction as exemplified by deuterium, and the details of nuclear structure, as illustrated by beryllium. As in the case of medium and heavy elements, the cross sections of other light elements investigated to date show the familiar giant dipole resonance behavior, and in some cases anomalous photon absorption has been reported in the form of "breaks" in the curve of bremsstrahlung yield *vs* maximum bremsstrahlung energy.<sup>1</sup>

Knowledge of the parameters of the giant resonance for light nuclei is, in fact, of importance in understanding the photon absorption mechanism in all nuclei, for the role played by subunits in the photoneuclear process can be investigated directly. The photodisintegration of helium is of importance in this respect.

For some light elements, the position of the resonance peak is far removed from the  $(\gamma, n)$  threshold, thus affording an opportunity for studying the photon absorption process over a wide energy region below the resonance. N<sup>14</sup>, with a  $(\gamma, n)$  threshold at 10.25 Mev and a dipole resonance peak at 22.5 Mev, is such a case.

Just as for other elements,<sup>2,3</sup> the direct detection of neutrons has many practical advantages over radio-

activity techniques for the measurement of the above reactions. There is the further advantage that the  $(\gamma, pn)$  thresholds are in some cases near the  $(\gamma, n)$  thresholds, and much of the neutron yield is lost if one relies on radioactivity. Since, however, it is often difficult to work with samples in the form of compounds when using neutron detection methods, we have modified the method to permit the use of gas targets, and report herein measurements made on helium, nitrogen, oxygen, neon, and argon. Fluorine does permit the use of the compound Teflon, since the neutron contribution from carbon can be separated with ease and the gas is somewhat more difficult to handle.

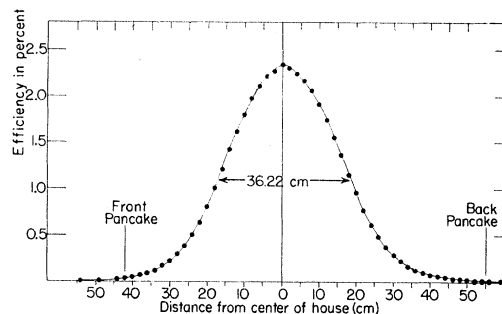


FIG. 2. Efficiency of apparatus for neutron detection as a function of position along beam axis.

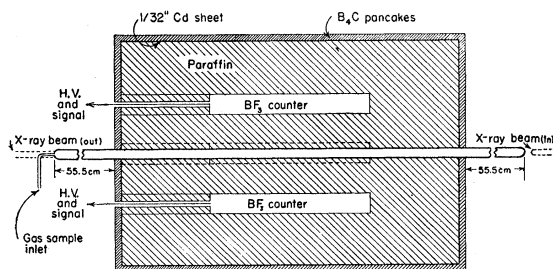


FIG. 1. Arrangement of paraffin block showing stainless steel cylinder to hold gaseous targets. The paraffin shielding (12 inches thick) that surrounds the entire block is not shown.

<sup>†</sup> Supported in part by the U. S. Air Research and Development Command and the joint program of the U. S. Office of Naval Research and the U. S. Atomic Energy Commission.

<sup>1</sup> Haslam, Katz, Horsley, Cameron, and Montalbetti, *Phys. Rev.* **87**, 196 (1952).

<sup>2</sup> R. Nathans and J. Halpern, *Phys. Rev.* **93**, 437 (1954).

<sup>3</sup> Montalbetti, Katz, and Goldemberg, *Phys. Rev.* **91**, 659 (1953).

### APPARATUS

The general arrangement of the apparatus as well as the significant performance data have been presented in previous publications.<sup>2</sup> The only modification for the present study was the introduction of the bomb to hold gases at high pressures, as shown in the diagram (Fig. 1) of the paraffin block used in these studies. The bomb, made from a 1½-in. o.d. stainless steel cylinder with 0.085 in. thick wall, fitted snugly into the beam hole passing through the paraffin house and extended approximately 25 cm beyond the shielding on both ends. The end caps, made from 0.049-in. stainless steel sheet drawn into hemispheres and welded to the tubing, were well outside the house so that  $(\gamma, n)$  reactions in the caps could not contribute appreciably to the background counts. The beam, 1.40 cm in diameter at the center of the house, did not of course strike the walls

of the bomb. The gases under study were led into the bomb from commercial cylinders through  $\frac{3}{16}$ -inch copper tubing soldered to the center of the rear cap. Neutron yields at varying bremsstrahlung energy were determined with the bomb flushed with nitrogen at one atmosphere as a standard background, and then with the gas to be measured added to the nitrogen to approximately 2000-lb/sq in. pressure.

With this arrangement neutrons from  $(\gamma, n)$  reactions in the gases originated along the beam for the full length of the house, as opposed to the situation with solid targets where the neutrons all originated from a target localized at the center of the house. Thus the neutron counting efficiency varied along the length of the target and required measurement. A 2-millicurie Ra-Be source was positioned at varying distances from the center of the apparatus along the beam axis, and the efficiency *vs* position thereby determined. The results are presented in Fig. 2, where the combined efficiency of the four counting channels for Ra-Be

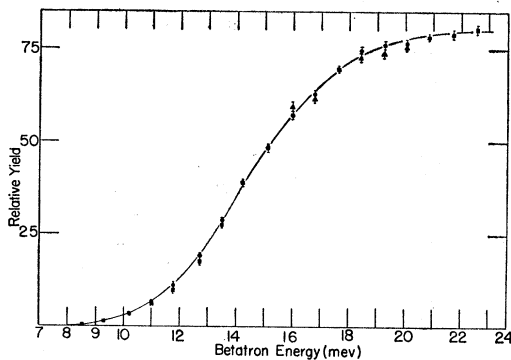


FIG. 3. Photoneutron yield from gold target. ● Gold at center of paraffin house; ▲ gold at end of house; ■ points common to both positions.

neutrons is plotted against distance of source from the center of the house. As indicated, the effective length of the gas targets was 36.22 cm.

Of greater concern than varying efficiency along the length of the targets, which affects only absolute values of  $(\gamma, n)$  cross sections, was the possibility that the detection efficiency for distances far from the center might be dependent on neutron velocity and thereby distort a yield curve since photoneutron velocity distributions change with increasing bremsstrahlung energy. Yield curves were therefore taken for a 498 mg/cm<sup>2</sup> gold target placed at the center of the house and at 25.1 cm from the center. Normalization of the yields as given by the relative efficiencies at the two positions, according to the results presented in Fig. 2, gave the two essentially identical yield curves of Fig. 3. It was therefore thought safe to assume that the counting efficiency was independent of neutron velocity throughout the length of the targets.

With the stainless steel bomb in the house, one further

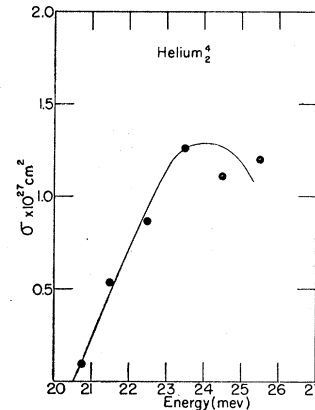


FIG. 4. Photoneutron excitation function for helium.

problem required investigation. Atomic scattering by the gaseous targets could cause a fraction of the scattered beam to strike the walls of the bomb and the resultant  $(\gamma, n)$  reaction in the iron might contribute to the measured net neutron yield attributed to the gaseous targets. Although this scattered radiation is degraded in energy, small-angle scattering is important for the forward portions of the target and the effect is enhanced by the low  $(\gamma, n)$  threshold of iron. This effect was easy to explore, however, for it should contribute a measured neutron yield at a betatron energy below the threshold of the element investigated but above the iron threshold. Helium and oxygen, with thresholds 9.3 Mev and 4.3 Mev, respectively, above the threshold for the 91.6 percent isotope of iron were carefully explored. A positive effect was measured, but it was found too small to influence in any way the cross-section curves derived from the measured yields.

Procedures for taking the photoneutron yield curves and converting to cross sections have been described in previous publications,<sup>2</sup> which also include details of operating conditions of the betatron used to produce the bremsstrahlung beam up to a maximum energy of 26 Mev.

## RESULTS

Cross section *versus* energy curves for all the elements investigated exhibited the familiar giant dipole resonance behavior with the possible exception of helium. In the latter element, the curve could not be explored over a sufficient range to be positive of the resonance, but indications are that helium is no exception. The parameters of the giant resonances as taken from the excitation functions are presented in Table I. Here  $E_m$  is the energy at the peak of the resonance,  $\sigma_m$  the value of the peak cross section,  $\Gamma$  the width at half-maximum, and  $\int \sigma dE$  the integrated cross section from threshold to 25 Mev. The details for each element are discussed below.

## HELIUM

The cross-section curve for helium is shown in Fig. 4, with the circles representing the values of the cross

TABLE I. Summary of data.

Element	Z	A	Percent abundance	Pressure lb/sq in.	$(\gamma, n)$	Thresholds in Mev			$E_m$ (Mev)	$\Gamma$ (Mev)	$\sigma_m$ (mb)	$\int \sigma dE$ (Mev-barns)
						$(\gamma, p)$	$(\gamma, pn)$	$(\gamma, 2n)$				
Helium	2	4	100	2190	20.6	19.8	25.9	28.1	24.0	—	1.3	0.004
Nitrogen	7	14	99.62	1820	10.5	7.6	12.4	31.3	22.5	3.2	15.3	0.061
		15	0.38									
Oxygen	8	16	99.76	2230	15.6	12.1	22.9	28.8	22.5	3.5	7.7	0.031
		17	0.04									
		18	0.20									
Fluorine	9	19	100	4.8 g/cm <sup>2</sup> Teflon	10.4	7.9	15.9	19.6	22.2	5.6	11.5	0.077
Neon	10	20	90.00	310	16.9	12.9	23.0	28.3	21.5	6.6	7.3	0.052
		21	0.27									
		22	9.73									
Argon	18	36	0.31	2100	9.8	11.1	20.0	14.9	20.0	8.5	31.2	0.23
		38	0.06									
		40	99.63									

section derived from the  $(\gamma, n)$  yield curve for helium by the method of successive bremsstrahlung subtractions. Since the peak of the resonance occurs at 24 Mev, it is difficult to tell how the curve behaves on the high side of the resonance, and values of  $\Gamma$  and  $\int \sigma dE$  are thus not known. The maximum cross section is measured to be 1.3 millibarns.

#### NITROGEN

Figure 5 represents the cross-section curve for nitrogen, a particularly interesting case both because of the large separation between the threshold (10.5 Mev) and the peak of the resonance (22.5 Mev) and because of the low value of the  $(\gamma, pn)$  threshold (12.4 Mev). The dotted curve represents the  $(\gamma, n)$  cross section as measured by Johns, Horsley, Haslam, and Quinton<sup>4</sup> using radioactivity. The large  $(\gamma, pn)$  contribution is clearly demonstrated, particularly since the  $(\gamma, 2n)$  threshold is at approximately 31 Mev and cannot contribute to the observed yields. The integrated cross section for total neutron yield is 0.06 Mev barn compared with the value of 0.015 Mev barn for the radio-

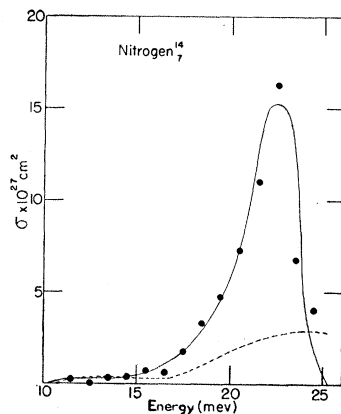


FIG. 5. Photoneutron excitation function for nitrogen.

<sup>4</sup> Johns, Horsley, Haslam, and Quinton, Phys. Rev. 84, 856 (1951).

activity data. The total neutron yield integrated cross section would be expected to include most of the contribution from the  $(\gamma, p)$  as well, for at energies in the vicinity of the rather narrow (3.2-Mev) resonance the emission of a proton is almost certain to be followed by neutron emission. It is clear that the radioactivity method gives erroneous values for the parameters of the dipole resonance.

#### OXYGEN

The oxygen excitation function is presented in Fig. 6. This does not represent a new result, as Montalbetti *et al.*<sup>3</sup> report a total neutron cross-section curve for oxygen as reproduced by the dotted curve of the figure. Here again the  $(\gamma, 2n)$  threshold (29 Mev) is far above the resonance position at 22.5 Mev. There may be a small  $(\gamma, pn)$  contribution starting at a threshold of 22.9 Mev.

#### FLUORINE

Fluorine was bombarded in the form of Teflon, with a composition of 76 percent fluorine and 24 percent carbon by weight. After subtraction of the known carbon yield from the total measured yield and calculation of a cross-section curve, the results are those

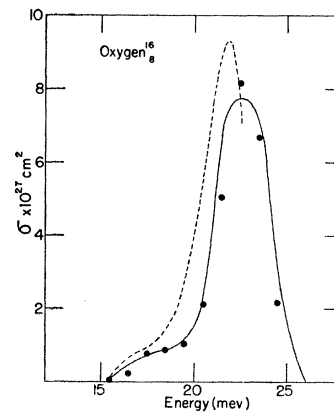


FIG. 6. Photoneutron excitation function for oxygen.

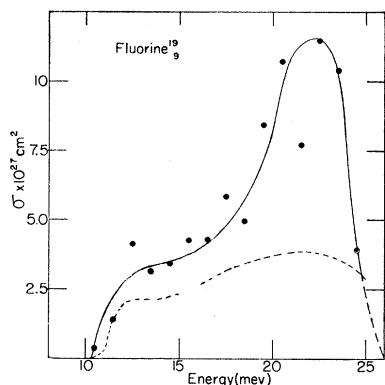


FIG. 7. Photoneutron excitation function for fluorine.

presented in Fig. 7. The dotted curve of the figure is that of Horsley, Haslam, and Johns<sup>5</sup> using radioactivity. The situation with fluorine is somewhat similar to that for oxygen. The  $(\gamma, pn)$  threshold is at 15.9 Mev. There is the one difference that the  $(\gamma, 2n)$  threshold at 19.6 Mev is below the peak.

NEON

The neon results plotted in Fig. 8 clearly show the two main isotopes, the 90 percent abundant Ne<sup>20</sup> isotope having a threshold of 16.9 Mev. The  $(\gamma, 2n)$  and  $(\gamma, pn)$  thresholds are too high to be of any significance. Ne<sup>20</sup> was considered important because of possible alpha-particle structure. In fact, the results of this paper for helium and oxygen and those for carbon<sup>2</sup> and the Be<sup>8</sup> core<sup>6</sup> of the Be<sup>9</sup> nucleus make interesting comparison with Ne<sup>20</sup>. This is illustrated in Fig. 9, where the cross section for each element is divided by the number of alpha particles and plotted *vs* energy.

ARGON

The total neutron cross-section curve for argon is shown in Fig. 10. The  $(\gamma, 2n)$  threshold is at 14.9 Mev

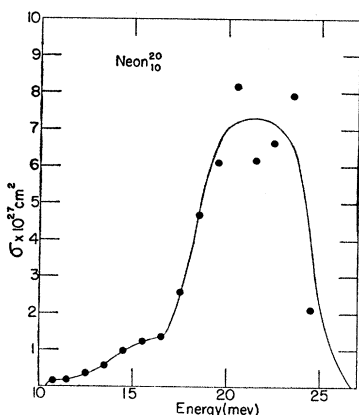


FIG. 8. Photoneutron excitation function for neon.

<sup>5</sup> Horsley, Haslam, and Johns, Phys. Rev. **87**, 756 (1952).  
<sup>6</sup> R. Nathans and J. Halpern, Phys. Rev. **92**, 940 (1953).

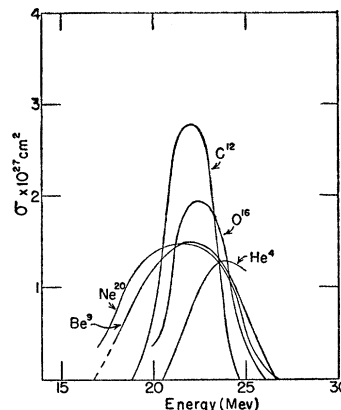


FIG. 9. Cross-section curves for alpha-particle nuclei. The cross-section curves for each element are divided by number of alpha particles and plotted against photon energy.

and the  $(\gamma, pn)$  at 20 Mev. An unambiguous separation cannot of course be made. The resonance width of 8.5 Mev and peak position of 20 Mev are consistent with values for other elements of comparable mass number.

DISCUSSION

It is doubtful that the various collective models proposed<sup>7-9</sup> to account for the giant photon absorption resonance in nuclei are applicable to light elements. Their chief prediction involves the dependence of the energy at the resonance maximum on atomic number. It should therefore be of interest to see how this energy for the elements herein reported compares with that for other elements. Figure 11 shows a plot of all such data from this laboratory. The solid curve drawn through the points represents a dependence of the form

$$E_m = 38.5A^{-0.19},$$

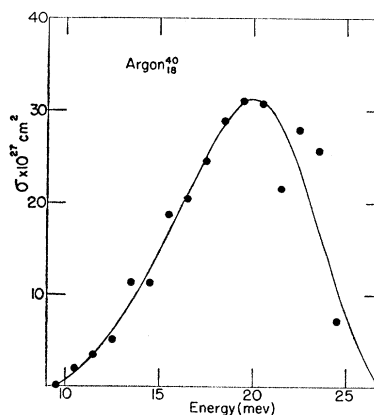


FIG. 10. Photoneutron excitation function for argon.

<sup>7</sup> M. Goldhaber and E. Teller, Phys. Rev. **74**, 1046 (1948).  
<sup>8</sup> Steinwedel, Jensen, and Jensen, Z. Naturforsch. **6a**, 218 (1951).  
<sup>9</sup> A. Reifman, Z. Naturforsch. **8a**, 505 (1953).

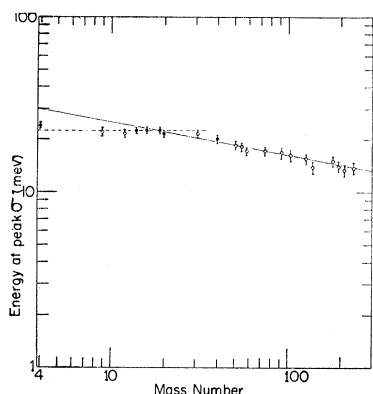


FIG. 11. Energy at giant resonance maximum vs mass number. The dots represent data of this paper. The circles are taken from the data of reference 2.

as previously reported.<sup>2</sup> Below an  $A$  of 30,  $E_m$  assumes a constant value of approximately 22.5 Mev.

Although a nuclear model should predict the width of the resonances as well as the peak energy, such calculations are at present not available. These involve the damping of any modes of oscillation induced by the incident photons. Figure 12 shows the dependence of the half-widths on mass number for all the elements of Fig. 11. Below a mass number of 30 the half-widths drop sharply below the trend for heavier elements as indicated by the solid line of the figure. The four anomalously low values above an  $A$  of 30 have been discussed previously.<sup>10</sup>

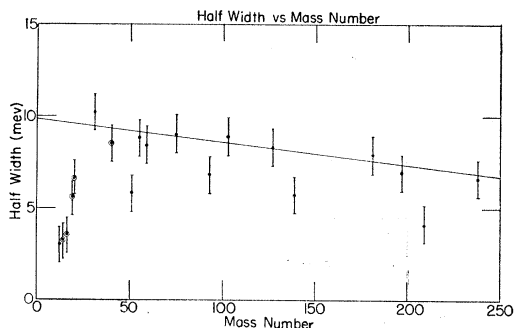


FIG. 12. Half-widths of the giant resonances as a function of mass number. The circles represent the data of this paper, the dots those of reference 2.

<sup>10</sup> R. Nathans and J. Halpern, Phys. Rev. **92**, 207 (1953).

The neutron integrated cross sections, on the other hand, depend only on the competition to neutron emission offered by other types of decay of the compound nucleus. Figure 13 represents the accumulated data on neutron integrated cross sections as a function of mass number, with the ordinate equal to the cross sections integrated to 25 Mev and divided by  $NZ/A$ . The horizontal lines of the figure correspond to limits imposed by the sum rules<sup>11</sup> for the integrated cross sections for dipole absorption summed over all partial reactions. Below a mass number of 50, other modes of decay of the compound nucleus become quite important.

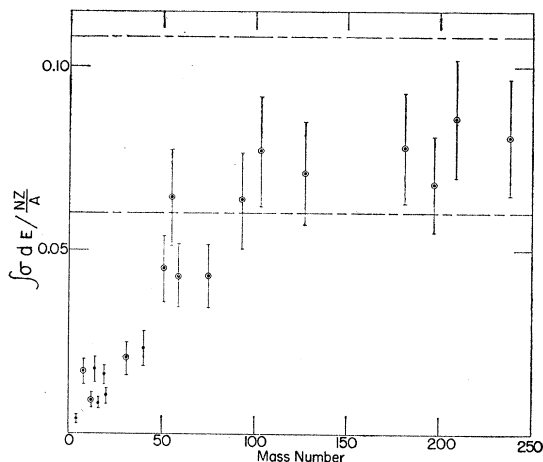


FIG. 13. Total neutron emission cross sections integrated to 25 Mev divided by  $NZ/A$  and plotted against mass number. The dots are the data of this paper, the circles those of reference 2.

In fact, as discussed previously for the case of carbon and beryllium,<sup>3</sup> addition of proton yield data will not be sufficient to bring the values into agreement with the sum rules unless one assumes large contributions to the yields by photons above an energy of 25 Mev. Nitrogen is another such example, for the measured integrated cross section for neutron emission includes most of the proton emission because of the importance of the  $(\gamma, pn)$  process. One should not overlook the possibility of large  $(\gamma, \gamma')$  processes below the particle emission thresholds.

<sup>11</sup> J. S. Levinger and H. A. Bethe, Phys. Rev. **78**, 115 (1950).